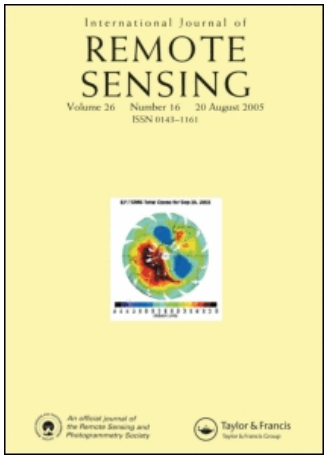

International Journal of Remote Sensing
Publication details, including instructions for authors and subscription information:
http://www.informaworld.com/smpp/title~content=t713722504

Geometrical modelling of soil bidirectional reflectance incorporating specular effects

J. Cierniewski [a]; F. Baret [b]; M. Verbrugghe [b]; J. F. Hanocq [b]; S. Jacquemoud [c]
[a] Institute of Physical Geography, Adam Mickiewicz University, Poznan, Poland
[b] INRA Bioctimatologie, Avignon, France
[c] Université Paris 7, Paris, France

Online Publication Date: 01 December 1996
To cite this Article: Cierniewski, J., Baret, F., Verbrugghe, M., Hanocq, J. F. and Jacquemoud, S. (1996) 'Geometrical modelling of soil bidirectional reflectance incorporating specular effects', International Journal of Remote Sensing, 17:18, 3691 - 3704
To link to this article: DOI: 10.1080/01431169608949178
URL: http://dx.doi.org/10.1080/01431169608949178

INT. J. REMOTE SENSING, 1996, VOL. 17, NO. 18, 3691–3704

Geometrical modelling of soil bidirectional reflectance incorporating specular effects

J. CIERNIEWSKI

Institute of Physical Geography, Adam Mickiewicz University, Fredry 10, 61-701 Poznan, Poland

F. BARET, M. VERBRUGGHE, J. F. HANOCQ

INRA Bioclimatologie, 84 914 Avignon, France

and S. JACQUEMOUD

Université Paris 7, 75 252 Paris, France

(*Received 24 October 1995; in final form 27 April 1996*)

Abstract. A geometrical model, taking into account the diffuse, as well as the specular component of energy leaving soil surfaces in the visible and near-infrared, is discussed here. The model computes the bidirectional reflectance of soils illuminated by a single source. A rough soil surface is simulated by equal-sized spheroids regularly spaced on a horizontal surface. The model was tested using soil bidirectional reflectance data obtained in laboratory conditions by Jacquemoud *et al* in 1992. Two parameters describing soil surface geometry were used for modelling the soil relative reflectance in laboratory conditions: the relative distance (d/a) between spheroids (relative to their horizontal radii (a)), and the shape of spheroids (b/a) (as proportion of their vertical (b) to horizontal radii (a)). The simulation of reflectance for soil surfaces of pebbles and sand, containing simple dense particles with rounded edges, can be carried out using the d/a and b/a ratios which nearly described their actual geometry. The reflectance of more geometrically complicated soil surfaces, such as clay and peat with irregular secondary porous aggregates, can be simulated by surfaces of effective geometry of vertically elongated spheroids.

1. Introduction

The geometry of the soil surface affects energy and water fluxes and the distribution of solar energy reflected from the surface. The reflectance of bare soils in the visible and near-infrared range has mainly been discussed as a background to the spectral response of vegetative surfaces (Brennan and Bandeen 1970, Kriebel 1976, Eaton and Dirmhirn 1979, Ott *et al.* 1984, Curran 1985, Bartlett *et al.* 1986, Milton and Webb 1987, Foody 1988). Rough soil surfaces usually show variation in brightness due to the direction of irradiation and also the direction from which reflectance is observed. The bidirectional character of soil surface reflectance has been explained by interactions between the directional component of solar irradiation and irregularities of the surface, i.e., soil aggregates, clods and soil microrelief configuration. These rough elements produce shadowing effects which change the amount and angular distribution of solar energy leaving the soil surface (Graetz and Gentle 1982, Cooper and Smith 1985, Norman *et al.* 1985, Ranson *et al.* 1985, Pech *et al.* 1986, Cierniewski 1987, Huete 1987, Milton and Webb 1987). In the absence of strong specular

behaviour, a soil surface seems to be the brightest from the direction which gives the lowest proportion of shaded fragments, the 'hot spot' direction. Hot spot features have been observed from *in situ* reflectance measurements of bare soils (Ott *et al.* 1984, Kimes and Sellers 1985, Milton and Webb 1987). The hot spot tends to be less pronounced when the solar zenith angle decreases. However, soil reflectance could clearly have also a forward scattering character due to specular reflection as observed on an alkali flat bare soil and a flat sand surface with uniform ripples composed of nearly pure gypsum crystals (Deering *et al.* 1990).

Most soil reflectance models that have been proposed focus on the hot spot description. The model of Norman *et al.* (1985) describes rough soil surfaces with aggregates and clods on the surfaces as cuboids of a given length, width and height situated on a horizontal plane. The plane and the cuboids are composed of the same smooth soil material with Lambertian scattering properties. The Monte Carlo reflectance soil surface model developed by Cooper and Smith (1985) assumes that the soil is a perfectly diffuse reflector at a microscopic level. In this case the probability that a photon will be scattered at a given angle only depends on the orientation of the soil surface. The soil surface irregularities were described by two microrelief forms whose height varies periodically according to a cosine function in one or two directions for 'row' and 'clump' soils, respectively. The diffuse character of the model causes rough soil surfaces to show the backscattering regime of the soil reflectance as the previous model. Hapke's (1981, 1984, 1986) models, developed for the interpretation of reflectance properties of planetary surfaces, produce BRDF signatures like those of a medium composed of particles characterized by a single-scattering albedo and a phase function.

The models take into account a parameter which depends upon regolith porosity and the particle size distribution. They are applicable to macroscopically rough surfaces, i.e., those with irregularities at scales larger than the wavelength of the radiation interacting with them. The macroscopic roughness causes shadowing at large phase angles and interparticle shadow hiding at small phase angles. The models have five input parameters. Jacquemoud *et al.* (1992) added a specular contribution and separated those parameters which depend on the wavelength (the single-scattering albedo) from those which were not wavelength-dependent. The model of Irons *et al.* (1992) describes the soil surface as made of uniform opaque spheres regularly spaced on an horizontal surface. Both direct and isotropically diffuse light illuminate the soil surface. The spheres and background are Lambertian. Soil reflectance is expressed as a function of the horizontal area shadowed by the spheres, the sunlit fraction, and the proportion of diffuse illumination, which depends on wavelength. These terms depend on the solar and view directions and on the characteristics of the simulated surface. Otterman's model (Deering *et al.* 1990) treats bare soil as thin vertical cylinders of variable heights with facet-reflectance and transmittance located randomly on an horizontal plane with Lambertian reflectance. Architecture of the soil protrusions are described by a parameter which is the sum of the height times diameter of these cylinders per unit horizontal area. The model assumes that the facet reflectance largely controls the backscatter while facet transmittance is responsible for determining forward scattering. This was the first model simulating both backscattering and forward scattering. It predicted a clear forward scattering character of reflectance for a surface with nearly pure gypsum crystals of high transmittance. Cierniewski and Verbrugghe (1994) developed a geometrical model simulating rough soil surface by equal-sized spheroids regularly spaced on an

horizontal plane. The model assumes that wave energy in the visible and the near-infrared range reflected from anisotropic soil surfaces is related to the fraction of sunlit soil surface. Furthermore, the energy leaving the sunlit soil fragments is directly proportional to the energy coming to them, that is, it also depends on the angle of incidence of the sunbeams on these directly illuminated parts. The model, tested on regularly spread pebbles of several centimetres diameter, shows its largest disagreement with the measurements in the forward scattering range. This was thought to be caused by the specular features of the soil reflection that were not taken into account in the modelling.

In this paper the initial geometrical model described by Cierniewski and Verbrugghe, 1994 is improved by adding a specular component and evaluated using soil bidirectional reflectance data obtained by Jacquemoud *et al.* (1992).

2. Methods

2.1. *The model*

This model computes the bidirectional reflectance of soils illuminated by a single source, i.e., no diffuse incident radiation is taken into account. This model computes only the single scattered reflectance. Equal-sized spheroids of horizontal (a) and vertical (b) radii, lying on a horizontal surface simulate the soil surface (figure 1). The spheres are regularly spaced at the distance d. The shaded and sunlit fragments of the structure are observed by a sensor within the r_f and the r_b radii of the basic area of the sensor which changes with the view zenith angle (θ_v) as:

$$r_f = r_b = 1/2 \; d \cos\theta_v. \tag{1}$$

Along these radii the model calculates segments of the sunlit (I) and shadowed fragments (S) of the given spheroid (Is, Ss), the adjoining spheroid (Ia, Sa), and the ground surface between the spheroids (Ig, Sg). The model divides the curvilinear slopes of the calculated sunlit soil surface segments into many (j) simple linear sub-slopes inclined at an angle β_i. The β_i angles in relation to the azimuth position of the soil slopes (ϕ_r), and angles of the source beam direction, θ_s and ϕ_s, determine the $E_{\beta i}$ factor that characterizes the energy reaching these sunlit fragments:

$$E_{\beta i} = \cos\theta_s \cos\beta_i + \sin\beta_i \sin\theta_s (\sin\phi_s \sin\phi_r + \cos\phi_s \cos\phi_r) \tag{2}$$

where ϕ_s is 90° for all solar azimuth angles.

The phase function that characterizes the spectral-diffuse scattering is assumed to have an ellipsoidal shape in the two-dimensional plane. The major radius of the ellipse (ae) and its minor radius (be) in an $x'y'$ coordinate system (figure 2) depend on the source zenith angle (θ_s) and sub-slope angle (β_i):

$$ae = [1/\cos(\theta_s - \beta_i)]^{0.5} \qquad be = 1. \tag{3}$$

Equation (3) was fitted to the specular behaviour of analysed soil surfaces in the tested illumination conditions. By rotating the $x'y'$ system with respect to the original xy one, using the following equations:

$$X_{ve} = be \cos(\beta_i + 90 - \theta_s - \theta_v) \qquad Y_{ve} = ae \sin(\beta_i + 90 - \theta_s - \theta_v), \tag{4}$$

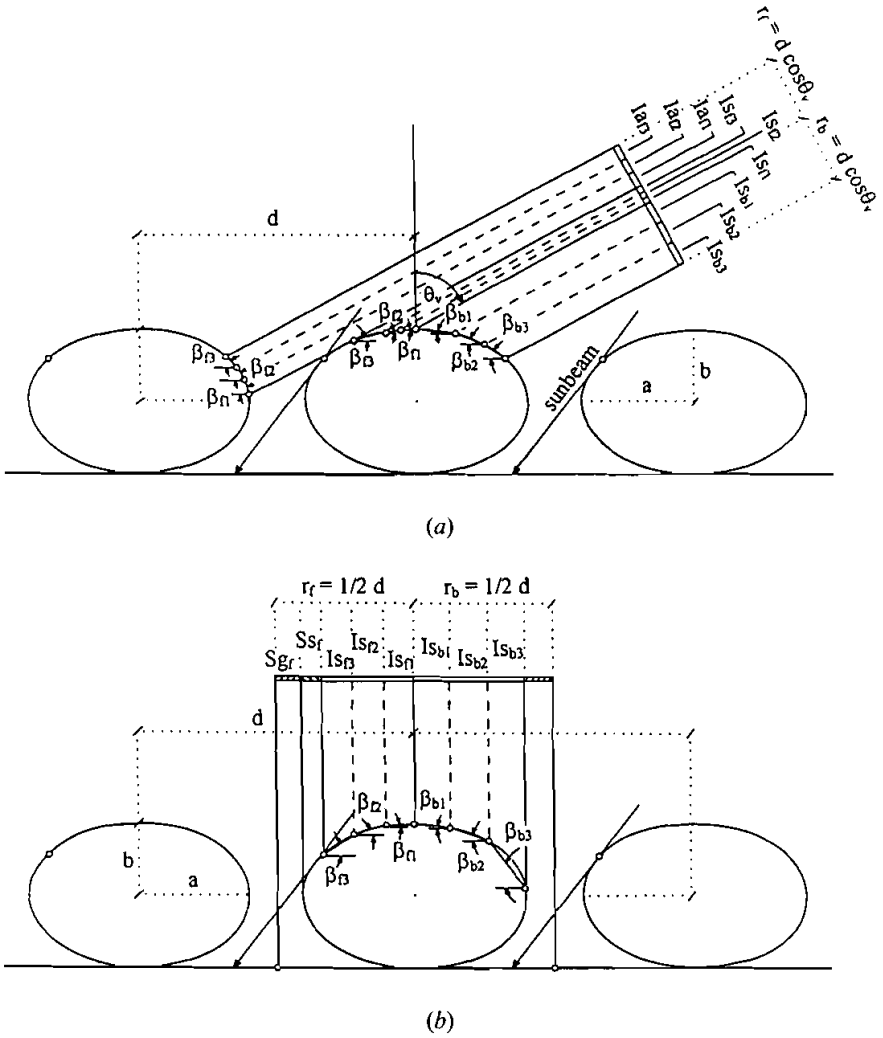

Figure 1. Geometry of the illuminated soil surface along the source principal plane with sunlit (I) and shaded (S) sub-segments of the given spheroid (Is, Ss), the adjoining spheroid (Ia, Sa) and the ground between the spheroids (Ig, Sg), situated at angles β_i. They are viewed from an off-nadir direction (*a*) and the nadir (*b*) within the basic view area defined by its r_f and r_b radii. θ_v is the view zenith angle.

we can find the position (X_{ve}, Y_{ve}) of the point of interaction of a given view direction (θ_v) with the ellipsoidal figure. So the magnitude of the soil spectral-diffuse vector (sdv) for the forward-scattering range may be written as:

$$\text{sdv} = (X_{ve}^2 + Y_{ve}^2)^{0.5} \tag{5}$$

and for the backscattering range the sdv = 1.

Assuming that the total energy leaving sunlit soil fragments is proportional to $E_{\beta i}$ multiplied by 'sdv', and to the length of sunlit soil sub-segments Ii, and that the energy leaving shaded fragments is zero, the radiance of the analysed soil surface (L) visible to the sensor from the given direction (θ_v) can be formulated

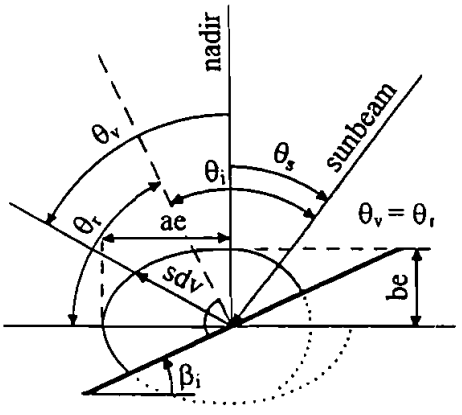

Figure 2. Distribution of the specular-diffuse vectors (sdv); ae and be are the major and the minor radius; θ_s is the source zenith angle; θ_v is the view zenith angle; θ_i is the incident angle, and θ_r is the angle of specular reflection.

as:

$$\left.\begin{aligned} &L = SE/SS; \\ &SE = \sum_{i=1}^{j} (Es_{\beta fi}\ sdv\ Is_{fi}) + \sum_{i=1}^{j} (Es_{\beta bi}\ sdv\ Is_{bi}) + \sum_{i=1}^{j} (Ea_{\beta fi}\ sdv\ Ia_{fi}) \\ &\qquad + \sum_{i=1}^{j} (Ea_{\beta bi}\ sdv\ Ia_{bi}) + Eg_f sdv\ Ig_f + Eg_b\ sdv\ Ig_b \\ &SS = Is_f + Ss_f + Is_b + Ss_b + Ia_f + Sa_f + Ia_b + Sa_b + Ig_f + Sg_f + Ig_b + Sg_b \end{aligned}\right\} \quad (6)$$

where subscripts 'f' and 'b' refer to the 'r_f' and 'r_b' radii of the basic view area, respectively.

The model calculates the radiance for the profile going through the centre of the spheroids, and then for several following profiles parallel to the first one, taking into account the variation of the ϕ_r angle. The total radiance (Lt) for a given view angle is computed as an average value from all the profiles and the flat space between the spheroids, where the radiance L for the flat plane equals $\cos\theta_s$.

The reflectance of the simulated surface is finally expressed by the relative reflectance factor (FR) defined as the proportion of the total radiance measured from an off-nadir direction $Lt_{(\theta)}$ to the radiance measured from the nadir $Lt_{(0)}$:

$$FR = Lt_{(\theta)}/Lt_{(0)} \quad (7)$$

The model predicts the reflectance factor of a horizontal soil surface viewed at a given zenith angle along the source principal plane relative to its nadir reflectance.

2.2. *Observed data*

The usefulness of the model in directional reflectance simulation of natural rough soil surfaces was tested using reflectance data obtained in laboratory conditions. We used the spectral data of 10 different dry samples collected by Jacquemoud *et al.* (1992): clay and peat with three roughness states, fine sand with two roughness states and pebbles. The data were measured on soil samples arranged in 50 cm square boxes. Five powerful halogen spotlights (2000 W) alternatively illuminated the

samples at zenith angles equal to 60°, 34° and 0° (nadir). We only used the data collected in the source principal plane by the Baringer HHRR radiometer, simulating the five TM channels (centre wavelengths: TM2 = 538 nm, TM3 = 631 nm, TM4 = 851 nm, TM5 = 1768 nm and TM7 = 2209 nm). The field-of-view of the instrument was 2·6° × 15·6°. In this work directional measurements were expressed as absolute reflectance, taken from 32 different positions (table 1).

2.3. *Fitting the model parameters to soil reflectance measurements*

The soil surface features determine the soil distribution of the reflectance. It is described in our model by two parameters: the relative distance between the spheroids (d/a) and the b/a ratio describing the flatness of the spheroids simulating soil aggregates. The soil reflectance distribution was calculated as the average value from 16 radiance profiles cutting the spheroid into equal spaces, and for the number of sunlit slope facets j = 8. The values of the d/a and b/a parameters were determined by a simple optimization technique. We computed the distances between the measured BRDF and the values simulated for a range of b/a (1 : 1 : 10) and d/a (1 : 0·5 : 6·5) parameter values. We then selected the couple of d/a and b/a values that provide the lowest r.m.s. figure 3 presents typical error surfaces for TM4 band. We tried to find the same d/a and b/a values for a given soil surface geometry for the five TM channels at three different source zenith angles: 60°, 34° and 0°.

3. Results

The simulated soil sample surfaces with the best fitted roughness parameters are presented in figure 4. The geometry of the soil surfaces, containing simple dense particles with rounded edges and not forming secondary aggregates, like the samples of pebbles and sand, is close to those simulated. The simulated surfaces form slightly flattened spheroids characterized by the b/a parameter equal to 0·75–0·85. The relative distance (d/a) between the regularly spaced spheroids simulating sand in the natural arrangement (moderately rough) is about 1·5 times higher than for its smooth state. The d/a distance for pebbles is nearly the same as for the moderately rough sand. In comparison with the clay and peat samples in the moderately and very rough states, sand in the moderately rough state and pebbles are characterized by considerably lower variation in the relative reflectance factor along the source principal plane (figure 5).

Without the artificial deformation of the soil aggregates describing the clay and peat surfaces, it would be impossible to model the directional reflectance from the soil samples. The vertical elongation of the simulated spheroids, replaces the more complicated geometry of the soil. The clay and peat surfaces contain particles very different in size and shape. They form secondary porous aggregates with not necessarily rounded edges. The highly irregular structure of peat is clearly visible in its

Table 1. Geometries of measurements for the bidirectional reflectance data. All measurements are performed in the principal plane.

Source (θ_s)	Zenithal position of sensor (θ_v)												
60	−70	−60	−45	−30	−15	0	15	30	40	45	50	65	70
34	−70	−55	−40	−34	−30	15	0	15	20	40	45	50	60
0	−60	−45	−30	−15	−10	−5	0						

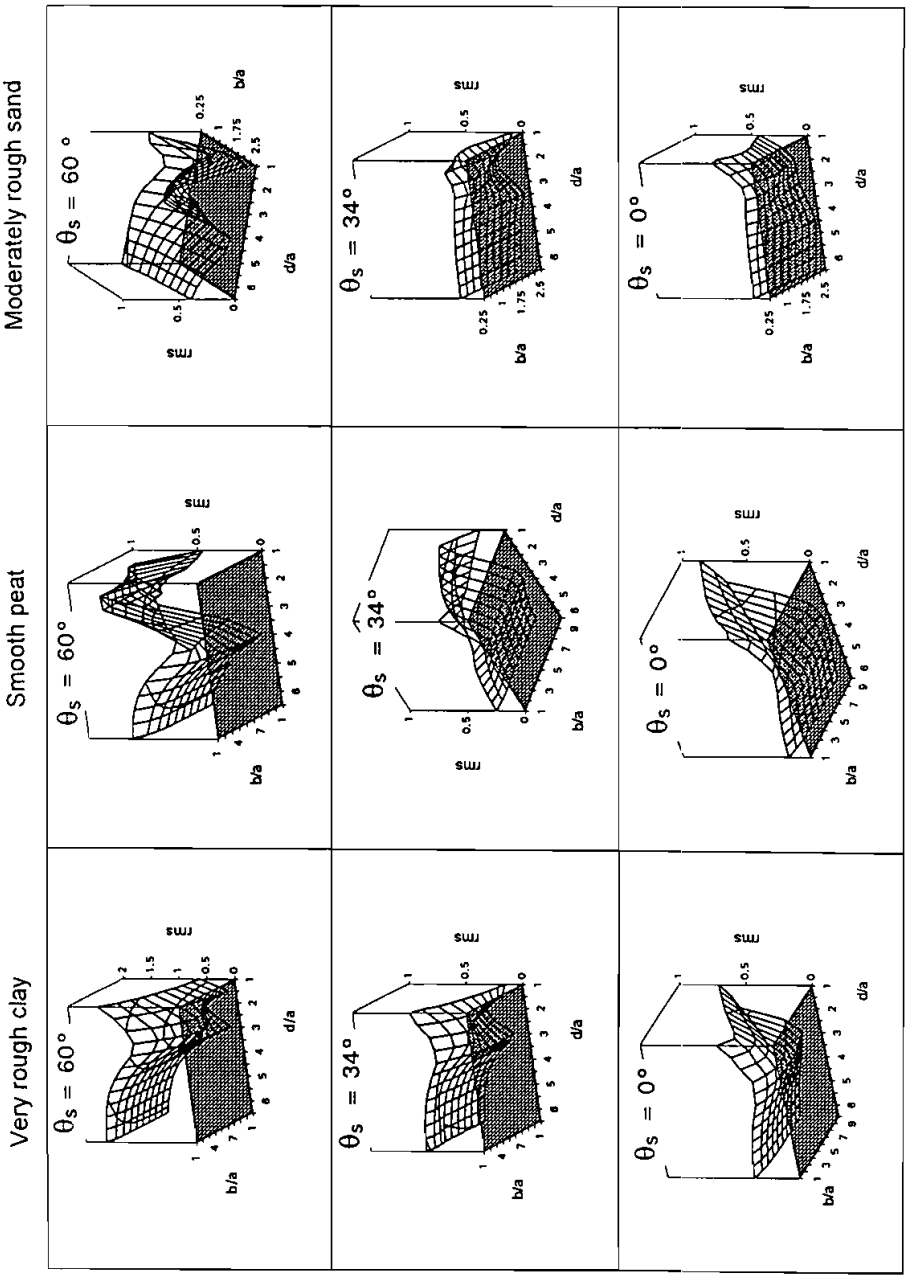

Figure 3. Typical distributions of the r.m.s. error computed between the simulated FR distributions and the measured FR reflectance data for the TM4 band along the source principal plane for a given solar zenith angle (θ_s). a and b are respectively the horizontal and vertical radii of the spheroids, and d is the distance between the spheroids.

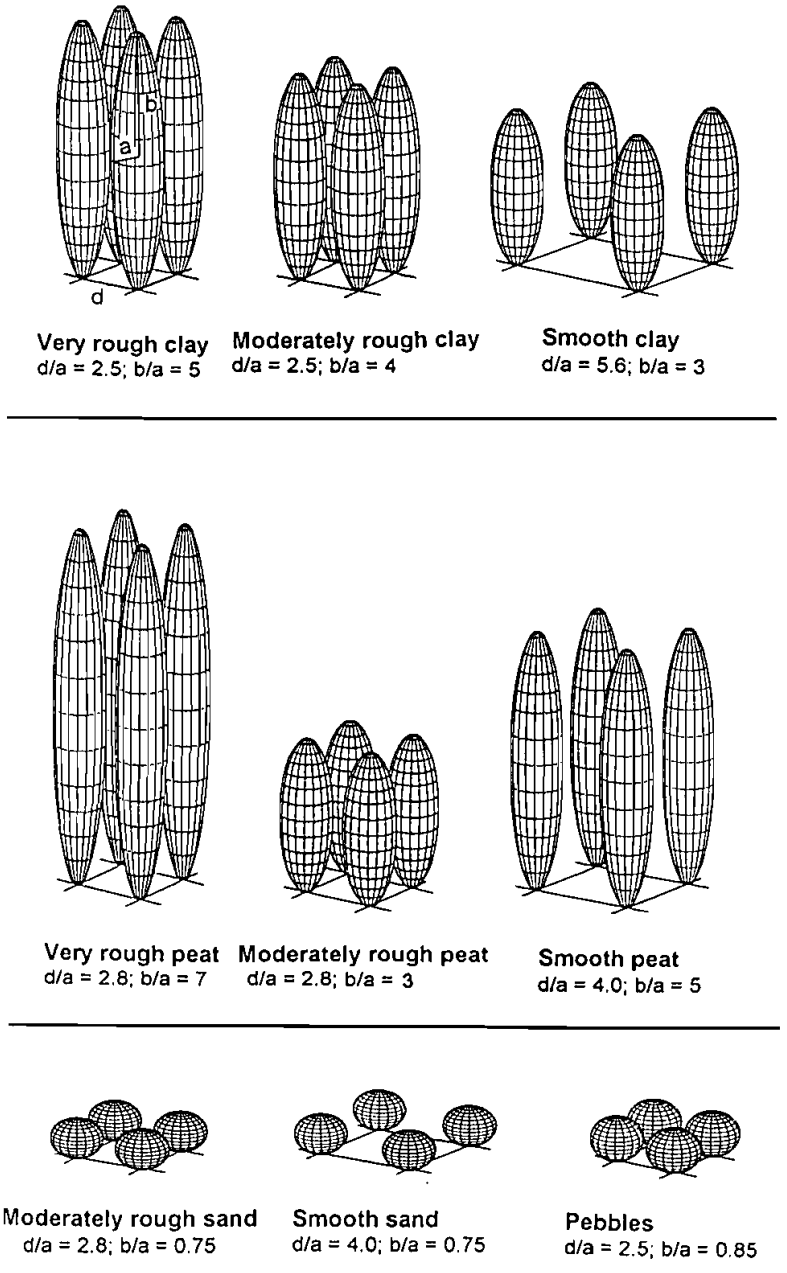

Figure 4. Simulated soil surfaces. a and b are respectively the horizontal and vertical radii of the spheroids, and d is the distance between the spheroids.

smooth sample. Thus, the artificial surfaces used for the simulation of the reflectance of the clay and peat samples are built with spheroids whose vertical axes are 3–7 times longer than their horizontal axes.

The accuracy of the simulated spectral data in relation to the measured ones was evaluated using linear regression analysis of the distribution of the soil relative reflectance factor along the source principal plane (SPP) simulated by the model

Table 2. Coefficient of determination (r^2) and (r.m.s.) error for measured and simulated reflectance data generated with (+spe) and without (−spe) specular reflectance effects.

	r^2		r.m.s.	
Channel	+spe	−spe	+spe	−spe
TM2	0·946	0·928	0·172	0·190
TM3	0·960	0·943	0·133	0·160
TM4	0·972	0·955	0·105	0·139
TM5	0·964	0·947	0·141	0·184
TM7	0·962	0·940	0·133	0·180

compared with that measured by the Barringer radiometer. The analysis was performed separately for the five channels using 351 pairs of data representing all the soil samples in different roughness states and illumination conditions (figure 6). It yielded similar values of coefficient of determination, between 0·95 and 0·97 for all the channels. The relative reflectance factor was predicted by the simulated surfaces with a mean deviation (r.m.s.) error from the measured reflectance data of about 0·10–0·17. By comparing these statistical parameters with analogous ones, but referring to simulated data without the generation of specular reflectance effects (table 2), we demonstrate the improvement in simulating real soil BRDF data when specular reflectance is added to the model simulation.

The coefficient of determination (r^2) and r.m.s. error, referring to the data generated with specular reflectance effects, computed separately for each of the analysed soil roughness states, are presented in table 3. For all samples except those representing smooth clay and sand the goodness-of-fit as expressed by the r^2 coefficient is between 87 per cent and 98 per cent. For the smooth samples the r^2 value is lower and is between 57 per cent and 76 per cent. This poorer goodness-of-fit is compensated for by the smaller difference in their relative r.m.s. error between the simulated and the reflectance data. The r.m.s. error for these smooth samples for all the channels is not higher than 0·12. Pebbles and sand in a moderately rough state have similarly low values of r.m.s. error. The highest relative r.m.s. errors were obtained for peat samples at three roughness levels (0·10–0·21) and for clay at two roughness levels (0·12–0·24). However, these r.m.s. values are compensated by the wide variation in the relative reflectance factor along the source principal plane (figure 5).

4. Conclusions

The model presented in this work can be used to describe the directional relative reflectance factor of natural soil materials with specular reflectance features along the principal plane. The model taking into account specular reflectance effects gives a better fit to the measured reflectance data than the earlier one (Cierniewski and Verbrugghe 1994), which simulates direct soil reflectance without specular effects.

Two parameters describing soil surface geometry were used for modelling the soil relative reflectance in laboratory conditions: the relative distance between spheroids (d/a) and the ratio describing their shape (b/a) simulating the soil aggregates and clods. The simulation of reflectance for soil surfaces like pebbles and sand, containing simple dense particles with rounded edges not forming secondary aggregates, can be carried out using the d/a and b/a ratios which nearly describe their actual geometry. These surfaces consist in flattened spheroids lying on an horizontal

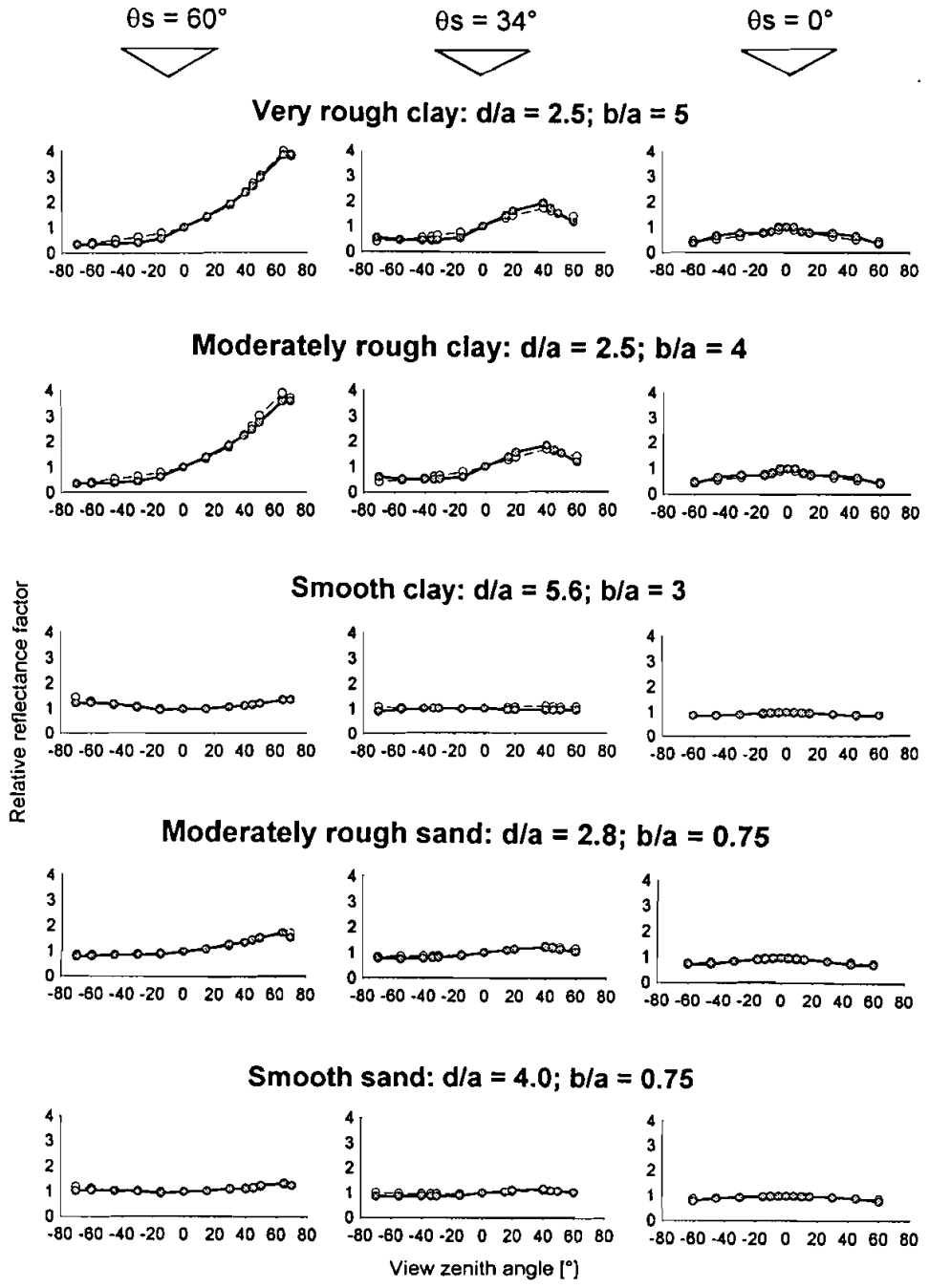

Figure 5. Relation between the relative reflectance factor along the source principal plane for TM4 predicted by the model (solid line) and that measured (dashed line) for a solution of soil samples. Negative angle values correspond to forward scattering directions and positive values, to backscattering directions.

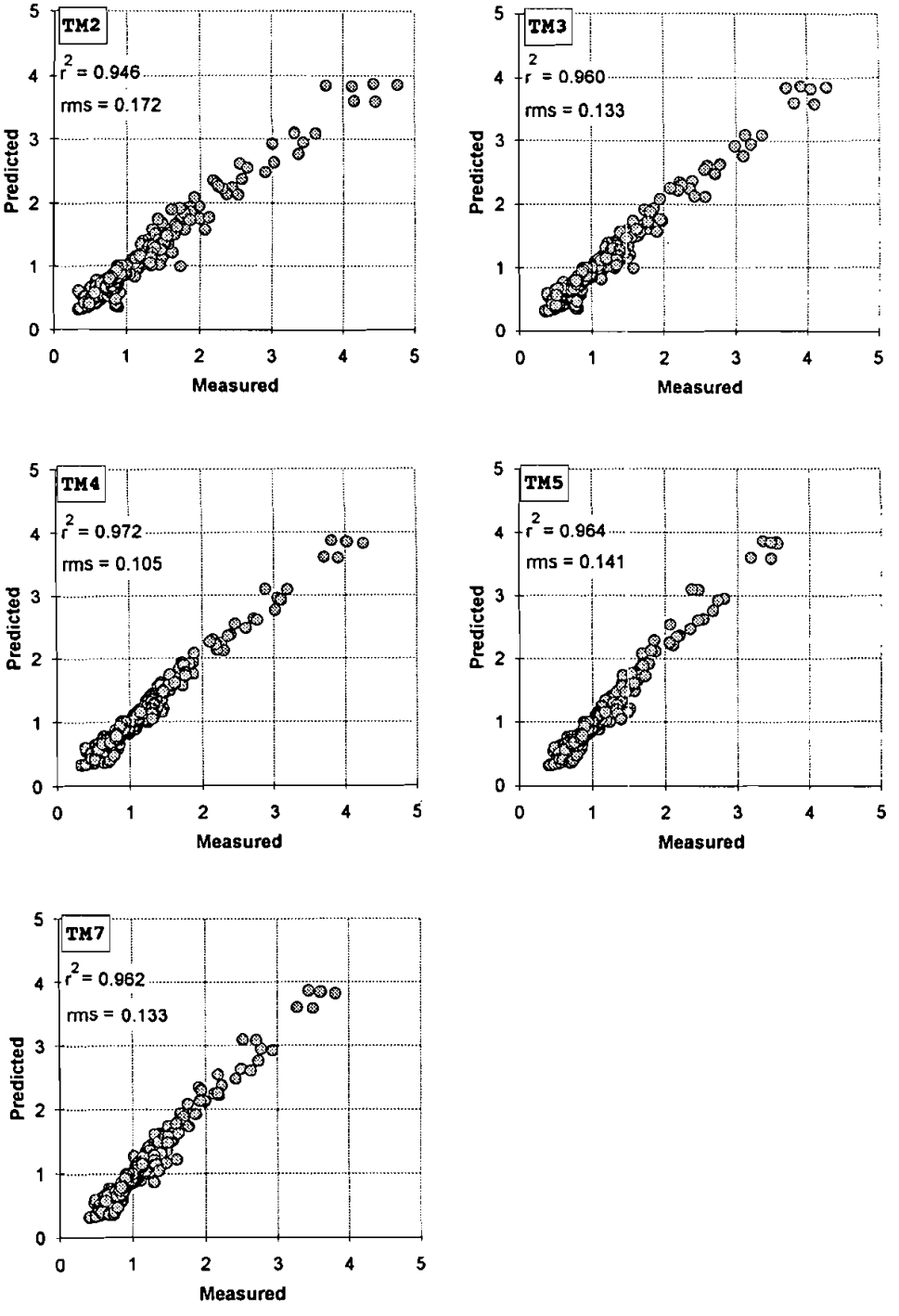

Figure 6. Relation between measured and predicted soil reflectance factors for wavelengths corresponding to the five channels: TM2, TM3, TM4, TM5 and TM7.

Table 3. Coefficient of determination (r^2) and r.m.s. error for measured and simulated reflectance data for different soil samples.

			TM2		TM3		TM4		TM5		TM7	
Material	d/a	b/a	r^2	r.m.s.	r^2	r.m.s.	r^2	r.m.s.	r^2	r.m.s.	r^2	r.m.s.
Very rough clay	2·5	5	0·976	0·240	0·980	0·145	0·982	0·124	0·980	0·176	0·983	0·168
Moderately rough clay	2·5	4	0·977	0·236	0·980	0·162	0·981	0·129	0·979	0·153	0·980	0·143
Smooth clay	5·6	3	0·762	0·120	0·752	0·097	0·754	0·078	0·634	0·086	0·565	0·100
Very rough peat	2·8	7	0·957	0·185	0·970	0·159	0·979	0·148	0·983	0·169	0·975	0·160
Moderately rough peat	2·8	3	0·931	0·211	0·948	0·169	0·968	0·141	0·965	0·250	0·959	0·220
Smooth peat	4·0	5	0·870	0·201	0·919	0·189	0·965	0·096	0·951	0·108	0·929	0·108
Moderately rough sand	2·8	0·75	0·942	0·130	0·943	0·091	0·953	0·063	0·950	0·086	0·954	0·088
Smooth sand	4·0	0·75	0·764	0·089	0·742	0·072	0·770	0·065	0·695	0·079	0·617	0·081
Pebbles	2·5	0·85	0·959	0·088	0·947	0·091	0·959	0·079	0·944	0·098	0·956	0·088

plane. The reflectance of more geometrically complicated soil surfaces such as clay and peat with irregular secondary porous aggregates, can be simulated by surfaces of effective geometry of vertically elongated spheroids.

Linear regression analysis showed the best agreement between the model-generated reflectance data and the measurements for pebbles and sand, with the least complicated surface geometry.

A third parameter, defining the ratio between the radiance of the shaded soil surface and the radiance of the same surface directly illuminated, would be necessary for modelling the soil relative reflectance in the field.

References

BRENNAN, B. and BANDEEN, W. R., 1970, Anisotropic reflectance characteristics of natural Earth surfaces. *Applied Optics*, **9**, 404–412.

BARTLETT, D. S., JOHNSON, M. A. and KLEMAS, V., 1986, Assessing impacts of off-nadir observation on remote sensing of vegetation: use of the Suits model. *International Journal of Remote Sensing*, **7**, 247–264.

CIERNIEWSKI, J., 1987, A model for soil surface roughness influence on the spectral response of bare soils in the visible and near-infrared range. *Remote Sensing of Environment*, **123**, 97–115.

CIERNIEWSKI, J., 1989, The influence of the viewing geometry of bare rough soil surfaces on their spectral response in the visible and near-infrared range. *Remote Sensing of Environment*, **127**, 135–142.

CIERNIEWSKI, J. and VERBRUGGHE, M., 1994, A geometrical model of soil bidirectional reflectance in the visible and near-infrared range. *Sixth International Symposium on Physical Measurements and Signatures in Remote Sensing, Actes Proceedings Val d'Isere, France*, 17–21 January, 1994, edited by International Society for Photogrammetry and Remote Sensing (Commission VII, Working Group 1), pp. 635–642.

COOPER, K. D. and SMITH, J. A., 1985, A Monte Carlo reflectance model for soil surfaces with three-dimensional structure. *I.E.E.E. Transations on Geoscience and Remote Sensing*, **23**, 668–673.

CURRAN, P. J., 1985, Earth surface interaction with electro-magnetic radiation. In *Principles of Remote Sensing* (London and New York: Longman).

DEERING, D. W., ECK, T. F. and OTTERMAN, J., 1990, Bidirectional reflectances of selected desert surfaces and their three-parameter soil characterization. *Agricultural and Forest Meteorology*, **52**, 71–93.

EATON, F. D. and DIRMHIRN, I., 1990, Reflected irradiances of natural surfaces and their effect on albedo. *Applied Optics*, **18**, 994–1003.

FOODY, G. M., 1988, The effects of viewing geometry on image classification. *International Journal of Remote Sensing*, **9**, 1909–1915.

GRAETZ, R. D. and GENTLE, M. R., 1982, A study of the relationship between reflectance characteristics in the Landsat wavebands and the composition and structure of an Australian semi-arid rangeland. *Photogrammetric Engineering and Remote Sensing*, **148**, 1721–1736.

HAPKE, B., 1981, Bidirectional reflectance spectroscopy 1. Theory. *Journal of Geophysical Research*, **86**, 3039–3054.

HAPKE, B., 1984, Bidirectional reflectance spectroscopy 3. Correction for macroscopic roughness. *Icarus*, **59**, 41–59.

HAPKE, B., 1986, Bidirectional reflectance spectroscopy 4. The extinction coefficient and the opposition effect. *Icarus*, **67**, 264–280.

HUETE, A. R., 1987, Soil and sun angle interactions on partial canopy spectra. *International Journal of Remote Sensing*, **18**, 1307–1317.

IRONS, J. R., CAMPBELL, G. S., NORMAN, J. M., GRAHAM, D. W. and KOVALICK, W. M., 1992, Prediction and measurement of soil bidirectional reflectance. *I.E.E.E. Transations on Geoscience and Remote Sensing*, **30**, 249–260.

JACQUEMOUD, S., BARET, F. and HANOCQ, J. F., 1992, Modelling spectral and bidirectional soil reflectance. *Remote Sensing of Environment*, **41**, 123–132.

KIMES, D. S. and SELLERS, P. J., 1985, Inferring hemispherical reflectance of the Earth's surface for global energy budget from remotely sensed nadir or directional radiance values. *Remote Sensing of Environment*, **118,** 205–223.

KRIEBEL, K. T., 1976, On the variability of the reflected radiation field due to differing distributions of the radiation. *Remote Sensing of Environment*, **4,** 57–264.

MILTON, E. J. and WEBB, J. P., 1987, Ground radiometry and airborne multispectral survey of bare soils. *International Journal of Remote Sensing*, **18,** 3–14.

NORMAN, J. M., WELLES, J. M. and WALTER, E. A., 1985, Contrast among bidirectional reflectance of eaves, canopies, and soils. *I.E.E.E. Transations on Geoscience and Remote Sensing*, **23,** 659–667.

OTT, W., PFEIFFER, B. and QUIEL, F., 1984, Directional reflectance properties determined by analysis of airborne multispectral scanner data and atmospheric correction. *Remote Sensing of Environment*, **116,** 7–54.

PECH, R. P., GRAETZ, R. R. and DAVIS, A. W., 1986, Reflectance modelling and the derivation of vegetation indices for an Australian semi-arid shrubland. *International Journal of Remote Sensing*, **17,** 389–403.